

Surface dimerization induced CuPt B versus CuPt A ordering of GaInP alloys

S. B. Zhang, Sverre Froyen, and Alex Zunger

Citation: *Applied Physics Letters* **67**, 3141 (1995); doi: 10.1063/1.114860

View online: <http://dx.doi.org/10.1063/1.114860>

View Table of Contents: <http://scitation.aip.org/content/aip/journal/apl/67/21?ver=pdfcov>

Published by the *AIP Publishing*

Articles you may be interested in

[Hydrogen-induced reconstruction of the GaP\(001\) surface studied by scanning tunneling microscopy](#)
J. Vac. Sci. Technol. B **14**, 3599 (1996); 10.1116/1.588733

[Correlation between surface structure and ordering in GaInP](#)
J. Vac. Sci. Technol. B **14**, 3013 (1996); 10.1116/1.589057

[Surface photoabsorption study of the effects of growth temperature and V/III ratio on ordering in GaInP](#)
J. Appl. Phys. **79**, 6895 (1996); 10.1063/1.361430

[Surface photoabsorption study of the effect of substrate misorientation on ordering in GaInP](#)
Appl. Phys. Lett. **68**, 2237 (1996); 10.1063/1.115870

[Surface photoabsorption study of the effect of V/III ratio on ordering in GaInP](#)
Appl. Phys. Lett. **68**, 1796 (1996); 10.1063/1.116016

Frustrated by old technology? Is your AFM dead and can't be repaired? Sick of bad customer support?

It is time to upgrade your AFM
Minimum \$20,000 trade-in discount for purchases before August 31st

Asylum Research is today's technology leader in AFM

dropmyoldAFM@oxinst.com

OXFORD INSTRUMENTS
The Business of Science®

Surface dimerization induced CuPt_B versus CuPt_A ordering of GaInP alloys

S. B. Zhang, Sverre Froyen, and Alex Zunger
National Renewable Energy Laboratory, Golden, Colorado 80401

(Received 12 June 1995; accepted for publication 10 September 1995)

Using a valence force field approach and *ab initio* pseudopotential calculations, we examine the role of subsurface strain in the ordering of $\text{Ga}_{0.5}\text{In}_{0.5}\text{P}$ alloys. We show that depending on the orientation of the surface phosphorus dimers, these alloys can have (i) a CuPt_A ordering for 1×2 or $c(4\times 4)$ reconstruction; (ii) a CuPt_B ordering for 2×1 or $\beta 2(2\times 4)$ reconstruction; and (iii) a triple period ordering for 2×3 or $c(8\times 6)$ reconstruction. These results are in good agreement with recent experiments of Gomyo *et al.* [Phys. Rev. Lett. **72**, 673 (1994); Jpn. J. Appl. Phys. **34**, L469 (1995)]. © 1995 American Institute of Physics.

Spontaneous ordering of III–V alloys has now been extensively observed and characterized in many semiconductors.¹ The most frequently seen spontaneous ordering consists of monolayer superlattice alternation along the $\langle 111 \rangle$ cubic body diagonals.¹ Of the four bulk-equivalent body diagonals, ordering has been seen to take place along only two directions ($[\bar{1}11]$ and $[1\bar{1}1]$, called CuPt_B variants), while, until recently, ordering along the other two directions ($[111]$ and $[\bar{1}\bar{1}1]$, called CuPt_A variants) was absent. Theoretical studies^{2–4} have demonstrated the relationship between surface reconstruction and spontaneous ordering in the 2D surface plane. It was shown that a cation-terminated 2×2 surface reconstruction leads to a 2D CuPt_B ordering in the top surface layer and in the fourth subsurface layer, while an anion-terminated 2×1 reconstruction leads to strong CuPt_B ordering in the third subsurface layer. The occurrence of ordering in these layers, depending on reconstruction type, illustrates the intimate relation between top surface growth morphology and the depth of the ordering layer. It was further shown⁴ that the main thermodynamic driving force for ordering is the creation of a subsurface selectivity for occupation by a small atom (Ga) *under* the strained dimer rows, and occupation by a large atom (In) underneath the opening *between* dimer rows. This subsurface selectivity induced by the top surface dimers depends naturally on the *dimer orientation*. The latter changes with reconstruction pattern. The subsurface selectivity in a given layer further depends on the depth of this layer under the top surface. Thus, nonflat surfaces can have a corresponding range of depths of subsurface ordering.

Several significant experimental observations were recently made in this respect. First, Gomyo *et al.*⁵ discovered, under MBE growth conditions favoring an anion-rich 2×3 surface reconstruction, a *triple period ordering* of $\text{Al}_{0.48}\text{In}_{0.52}\text{As}/\text{InP}(001)$, in *either* the $[111]$ or the $[\bar{1}\bar{1}1]$ directions. Philips *et al.*⁶ recently also observed, in (001) $\text{In}_{0.53}\text{Ga}_{0.47}\text{As}$ MBE epilayers, a triple period ordering in *two* directions: $[111]$ and $[\bar{1}\bar{1}1]$. Second, Gomyo *et al.*⁷ discovered a CuPt_A ordering of $\text{Al}_{0.5}\text{In}_{0.5}\text{P}/\text{GaAs}(001)$ under MBE growth conditions favoring an *anion-terminated* 2×2 reconstruction (with 1×2 basic building blocks). In contrast, the conventional higher growth temperature $T\sim 560^\circ\text{C}$ produces the 2×1 reconstruction that leads to CuPt_B ordering.^{1,5} Both the 2×2 and 2×3 surface reconstructions occur at low

growth temperatures (520°C for 2×2 and 415 and 460°C for 2×3 , respectively) and are hence believed to be more anion-rich than the 2×1 surface. Such reconstructions with heavy excess (>1 monolayer) of anions were not studied theoretically before since the nature of the surface structure under heavy anion coverage has become clear only recently.⁸ In this letter, we show via total energy minimization that (i) the anion-terminated 2×1 surface reconstruction stabilizes 2D CuPt_B ordering of the $\text{Ga}_{0.5}\text{In}_{0.5}\text{P}$ alloy by 88 meV/surface atom; (ii) the 1×2 double P layer reconstruction (a simplified version of the 2×2 reconstruction) stabilizes CuPt_A ordering by 155 meV/surface atom while (iii) the 2×3 surface stabilizes a triple-period ordering by 97 meV/surface atom. These large stabilization energies are predicted to lead to a significant ($\sim 60\%$) degree of ordering at growth temperatures. Our results confirm the suggestion of Gomyo *et al.*^{5,7} via a thermodynamic theory.

We first concentrate on the main distinguishing features of various reconstructions^{5,7} [Fig. 1(a)]: observe that while both the 2×1 and the 1×2 surfaces are terminated by P dimers, due to the occurrence of double phosphorus layers in the 1×2 surface, its P–P dimers are rotated by 90° with respect to those of the 2×1 surface. The 2×3 surface, on the other hand, can be viewed as a combination of the 1×2 and 2×1 surfaces, the former occupying $2/3$ of the total projected surface area. We conducted elastic energy minimization calculations via a valence-force-field (VFF) model (Refs. 2 and 4 and references therein) on various ordered patterns on the model 2×1 , 1×2 , and 2×3 surfaces, thus establishing the basic relation between dimer orientation and type of stable ordering. Conclusions drawn from these calculations were then examined by more sophisticated first principles self-consistent calculations on realistic^{8–10} but complicated $\beta 2(2\times 4)$ and $c(4\times 4)$ surfaces, containing, respectively, the building blocks (or motifs) of the 2×1 and 1×2 model surfaces.

The total VFF elastic energy is minimized with respect to atomic displacements subject to the constraint that surface P–P dimers are fixed at the dimer geometry determined by self-consistent pseudopotential calculations.¹⁰ The contribution of all surface layer P–P dimer bonds is omitted from the elastic energy. We use as input to the VFF calculations the equilibrium bond lengths and force constants determined from first-principles pseudopotential calculations^{3,4} for zinc-

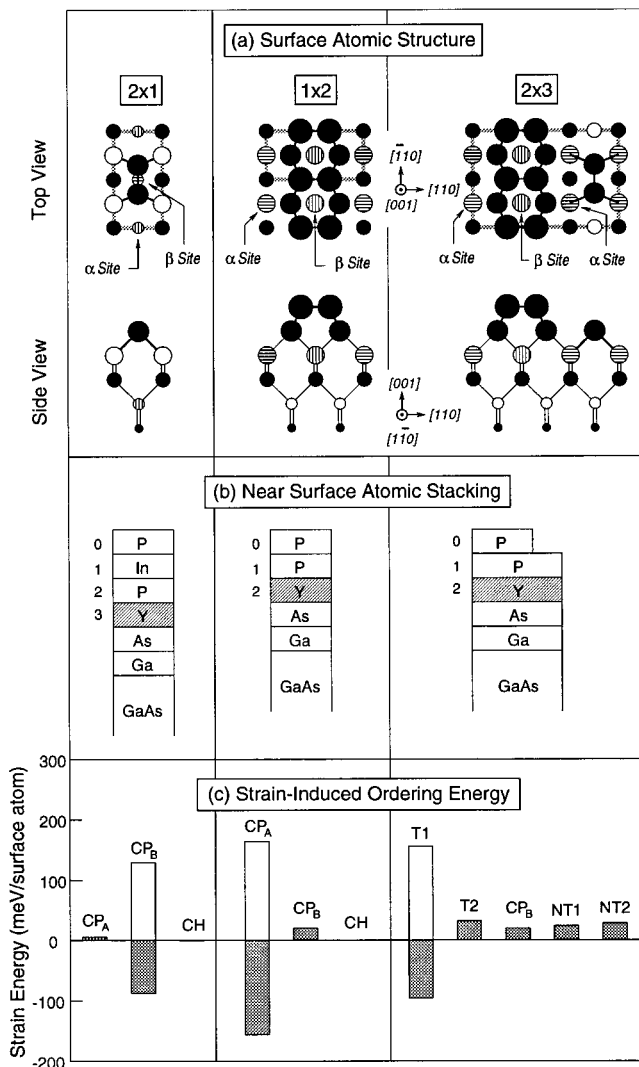


FIG. 1. (a) Top and side views of the 2×1 , 1×2 , and 2×3 model surface reconstructions. The filled and open circles indicate anion and cation sites, respectively, with sizes descending from top surfaces. The cation sites α (under the dimers) and β (between dimer rows) exhibit size selectivity. (b) Near surface atomic stacking sequences. Layer Y containing sites α and β is the most strained cation layer. (c) Calculated ordering energy (with respect to phase separation) in layer Y for various 2D occupation patterns given in Fig. 2. Here, $\text{CuPt}_A = \text{CuPt}_A$, $\text{CP}_B = \text{CuPt}_B$, CH-chalcopyrite, while T1, T2, NT1, and NT2 label the 2D occupation patterns of the 2×3 surface. Clear bars are used when swapping Ga with In atoms in a given pattern resulting in different energies.

blende GaP, InP, GaAs, and InAs. In the case of P double layers, we assume that the interlayer force constants involving surface P atoms (which assume the positions of cations in the normal zinc-blende stacking) and first subsurface layer P atoms (which assume the positions of anions in the zinc-blende stacking) are given by the average force constants of bulk zinc-blende GaP and InP. We have tested this assumption for the $c(4\times 4)$ surface by comparing to first-principles pseudopotential results. The agreement is within a few hundredth of an angstrom for atomic positions and a few meV/surface atom for energies for displacement amplitudes of $\leq 0.5 \text{ \AA}$.

Figure 1(c) shows the relative energies of various ordered 2D structures of $\text{Ga}_{0.5}\text{In}_{0.5}\text{P}$ (illustrated in Fig. 2)

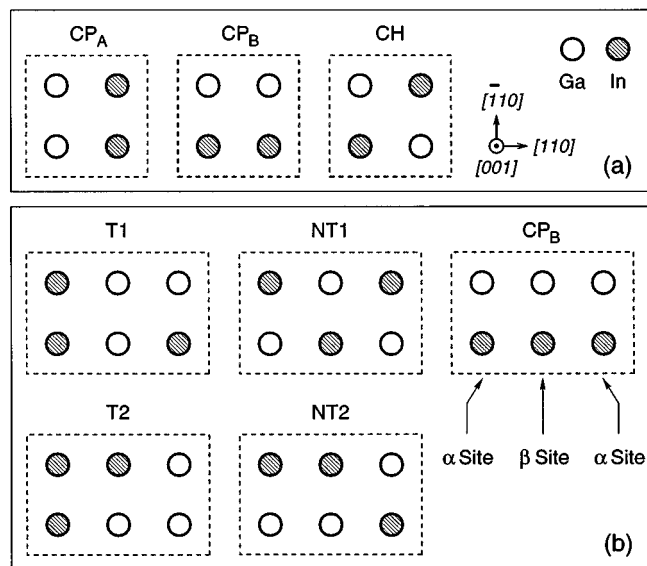


FIG. 2. Occupation patterns of Ga/In atoms for (a) the 2×1 and 1×2 surfaces and (b) the 2×3 surface. In (b), both T1 and T2 represent a three-period 2D ordering in the $[110]$ direction. A 50:50 Ga/In ratio is assumed.

placed at the Y =third, second, and second subsurface layer, respectively, for the 2×1 , 1×2 , and 2×3 surfaces. Negative energies in Fig. 1(c) mean stable structures. A 2×2 superperiodicity is used in Fig. 2(a) for the 2×1 and 1×2 surfaces, but not for the 2×3 surface. A primitive 2×3 surface cell has ten different occupation patterns. Some of them are degenerate. Here, we show in Fig. 2(b) the five nondegenerate patterns: T1, T2, CuPt_B , NT1, and NT2. Out of the five, only T1 and T2 may evolve into triple period ordering in the $[110]$ direction. We observe from Fig. 1 the following. (i) The 2×1 surface exhibits a strong CuPt_B ordering at the third subsurface layer (ordering energy $\Delta E_{\text{ord}}=88 \text{ meV/surface atom}$). The ordering direction is $[\bar{1}10]$, which is the dimerization direction of this surface. (ii) The 1×2 surface shows a strong CuPt_A ordering at the second subsurface layer with $\Delta E_{\text{ord}}=155 \text{ meV/surface atom}$. The ordering occurs along $[110]$, which is the dimerization direction of this surface. (iii) While in the 2×1 surface, the relaxation of the first subsurface layer has but a small effect on the ordering energy at Y =third subsurface layer,⁴ a much larger first subsurface layer relaxation effect occurs in the 1×2 surface that orders at the Y =second subsurface layer. This reflects the importance of atomic relaxations at the immediate vicinity of the ordered layer Y in minimizing strain energies. Without first subsurface layer relaxation, the ordering energy in the 1×2 surface is 287 rather than 155 meV/surface atom. (iv) The 2×3 surface shows a strong three-period ordering with $\Delta E_{\text{ord}}=97 \text{ meV/surface atom}$. The ordering direction is $[110]$, which coincides with the dimerization direction of the top layer of this surface.

Results (i), (ii), and (iv) are in good accord with recently suggested qualitative correlations between surface reconstruction and alloy ordering by Gomyo *et al.*^{5,7} Our calculations further establish a quantitative thermodynamic incentive for such correlations, which can be readily understood from surface geometries: anions are normally second nearest

neighbor atoms in their normal tetrahedral positions, but at the surface they form dimers and are thus displaced towards each other by a sizeable amount (~ 0.8 Å each). This creates a compressive strain on the subsurface layer atoms lying directly below the dimer rows [the cation site α in Fig. 1(a)], and a tensile strain on atoms underneath the opening between the dimer rows⁴ [i.e., the cation site β in Fig. 1(a)]. This undulating subsurface strain leads to a preference⁴ for a small atom (Ga) at the compressed site β and a large atom (In) at the expanded site α .

We will not pursue in this letter the question of layer stacking, i.e., 3D ordering as (a) this is not essential to explain CuPt_A vs CuPt_B ordering and (b) it involves many additional factors including surface steps that select the *sub-variants* of CuPt_A or those of CuPt_B. Recent pseudopotential calculation of surface formation energies versus phosphorus chemical potential¹⁰ suggested that only samples grown with heavy excessive surface P atoms would have the desired 1×2 or 2×3 structural pattern. This often requires low temperature growth as achieved by Gomyo *et al.*^{5,7}

More elaborate first-principles total energy calculations on realistic surfaces support the conclusions derived here from elastic energy calculations on model surfaces. Using a pseudopotential method, we have calculated the total energies for Ga_{0.5}In_{0.5}P surfaces with realistic surface reconstructions—the $\beta 2(2\times 4)$ reconstruction for single P layer 2×1 surface and the $c(4\times 4)$ reconstruction for the double P layer 1×2 surface. (Realistic surfaces have larger unit cell sizes than model surfaces, since the former have surface charge compensation requiring many atoms.) To compare the results of the first-principles and VFF calculations, we have calculated the respective order parameter η , which measures the degree of 2D ordering regardless of the details of surface reconstructions. In particular, we group all distinct cation sites in layer Y into two 2D sublattices $\{\alpha\}$ and $\{\beta\}$ along the ordering direction. Assuming that c_α and c_β are the indium concentrations of $\{\alpha\}$ and $\{\beta\}$, respectively, the order parameter is simply $\eta = c_\alpha - c_\beta$. If $c_\alpha = 1$, then $\eta = 1$, indicating perfect ordering. If, on the other hand, $c_\alpha = 0.5$, one would have $c_\beta = 0.5$, and thus $\eta = 0$, indicating perfect randomness. The model 2×1 and 1×2 surfaces are special cases where all sites on sublattice $\{\alpha\}$ are identical and all sites on sublattice $\{\beta\}$ are identical as shown in Fig. 1(a).

Here, we evaluate η at second and third subsurface layers for $c(4\times 4)$ and $\beta 2(2\times 4)$ surfaces, respectively, and correspondingly for the model 1×2 and 2×1 surfaces. The calculation was done following Osorio *et al.*⁴ by assigning an on-site energy $\Delta J_1^{(\alpha)}$ and finding its occupation probability $c_\alpha(T)$ using the Bragg–Williams method. Figure 3 shows that η derived from first-principles calculations with the $\beta 2(2\times 4)$ and $c(4\times 4)$ surface reconstructions follow the same trends (with smaller magnitude) as those derived from VFF calculations using the 2×1 and 1×2 surfaces. The smaller magnitude of η is expected as the more complicated reconstruction patterns of the realistic surfaces have defect-like surface features absent in the model surfaces that do not

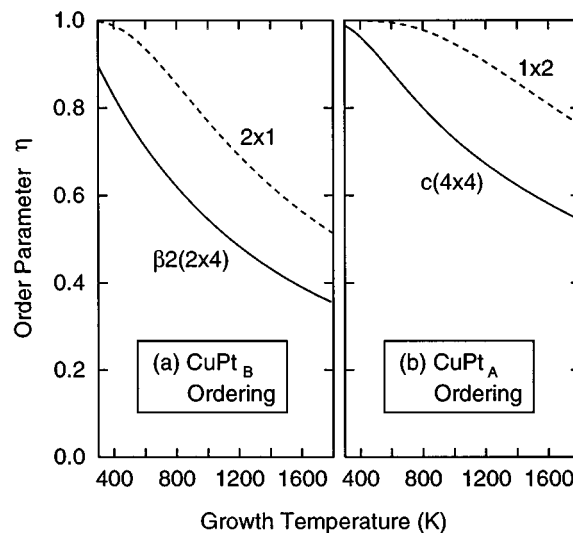


FIG. 3. Long-range order parameter η for (a) the $\beta 2(2\times 4)$ and 2×1 surfaces (Y =third subsurface layer) and (b) the $c(4\times 4)$ and 1×2 surfaces (Y =second subsurface layer), respectively. A 50:50 Ga/In ratio is assumed. Solid lines: first principles; dashed lines: VFF results.

serve to promote ordering energies. Figure 3 shows that both the pseudopotential and the VFF calculation predict a stronger 2D ordering for the double P layer [$c(4\times 4)$ and 1×2] surface than that of the single P layer [$\beta 2(2\times 4)$ and 2×1] surface.

In summary, we showed via thermodynamic energy minimization that the orientation of surface phosphorus dimers correlates with the type of ordering— CuPt_A, CuPt_B, and a triple period ordering—in Ga_{0.5}In_{0.5}P in good agreement with experiments.

We thank A. Gomyo and T. Suzuki for useful comments. This work was supported by the Office of Energy Research, Division of Materials Science, U.S. Department of Energy, under Contract No. DE-AC36-83-CH10093.

¹A. Zunger and S. Mahajan, in *Handbook of Semiconductors*, edited by S. Mahajan (Elsevier, Amsterdam, 1994), Vol. 3, p. 1399.

²J. E. Bernard, L. G. Ferreira, S. H. Wei, and A. Zunger, *Phys. Rev. B* **38**, 6338 (1988); J. E. Bernard, R. G. Dandrea, L. G. Ferreira, S. Froyen, S. H. Wei, and A. Zunger, *Appl. Phys. Lett.* **56**, 731 (1990).

³S. Froyen and A. Zunger, *Phys. Rev. Lett.* **66**, 2132 (1991).

⁴J. E. Bernard, S. Froyen, and A. Zunger, *Phys. Rev. B* **44**, 11178 (1991); R. Osorio, J. E. Bernard, S. Froyen, and A. Zunger, *Phys. Rev. B* **45**, 11173 (1992).

⁵A. Gomyo, K. Makita, I. Hino, and T. Suzuki, *Phys. Rev. Lett.* **72**, 673 (1994).

⁶B. A. Philips, I. Kamiya, L. T. Florez, D. E. Aspnes, S. Mahajan, and J. P. Harbison, *Phys. Rev. Lett.* **74**, 3640 (1995).

⁷A. Gomyo, M. Sumino, I. Hino, and T. Suzuki, *Jpn. J. Appl. Phys.* **34**, L469 (1995).

⁸M. D. Pashley, K. W. Haberern, W. Friday, J. M. Woodall, and P. D. Kirchner, *Phys. Rev. Lett.* **60**, 2176 (1988); H. H. Farrell and C. J. Palmstrom, *J. Vac. Sci. Technol. B* **8**, 903 (1990); D. K. Biegelsen, R. D. Bringans, J. E. Northrup, and L. E. Swartz, *Phys. Rev. B* **41**, 5701 (1990).

⁹J. E. Northrup and S. Froyen, *Phys. Rev. Lett.* **71**, 2276 (1993); J. E. Northrup and S. Froyen, *Phys. Rev. B* **50**, 2015 (1994).

¹⁰S. Froyen and A. Zunger *Phys. Rev. B* (in press).